Green Chemistry

Accepted Manuscript

ROYAL SOCIETY OF CHEMISTRY

www.rsc.org/greenchem

Journal Name

RSCPublishing

COMMUNICATION

Facile route to conformal hydrotalcite coatings over complex architectures: a hierarchically ordered nanoporous base catalyst for FAME production

Cite this: DOI: 10.1039/xoxxoooooox

Received ooth January 2012,
Accepted ooth January 2012

DOI: 10.1039/xoxxoooooox

www.rsc.org/

Julia J.Creasey,[a] Christopher M.A. Parlett,[b] Jinesh C. Manayil,[b] Mark Isaacs,[b] K. Wilson[b] and Adam F. Lee[*b]

An alkali- and nitrate-free hydrotalcite coating has been grafted onto the surface of a hierarchically ordered macroporous-mesoporous SBA-15 template via stepwise growth of conformal alumina adlayers and their subsequent reaction with magnesium methoxide. The resulting low dimensional hydrotalcite crystallites exhibit excellent per site activity for the base catalysed transesterification of glyceryl triolein with methanol for FAME production.

Rising global energy demand over the next 25 years, notably among emergent economies,[1] is driving the quest for sustainable routes to low cost, liquid transportation fuels from biomass feedstocks.[2] Around 9 % of transportation energy needs are predicted to be met via liquid biofuels by 2030.[3] The past decade has seen much criticism of first-generation bio-fuels derived from edible plant materials which are attributed to significant land use changes and deforestation in South East Asia.[4] In order for advanced bio-fuels to be considered truly sustainable, they must be sourced from non-edible crop components, forestry waste, alternative non-food plants such as switchgrass, Miscanthus or Jatropha curcas[5] which require minimal cultivation and do not compete with traditional arable land or drive deforestation, algal sources or the lignocellulosic components of municipal waste such as packaging materials.

Although there is burgeoning interest in extracting bio-oils from aquatic biomass, which can yield 80-180 times the annual volume of oil per hectare than plants,[6] process scale-up and the availability of nutrient resources remains challenging.[7] The biorefinery concept affords biomass the simplest and most popular approach to drop-in transportation fuels,[8] based upon carbohydrate pyrolysis and subsequent hydrodeoxygenation (HDO)[9] of the resulting bio-oils or their gasification and subsequent Fischer-Tropsch processing[10] to gasoline and diesel,[11] or lipid transesterification to biodiesel.[12] Catalytic depolymerisation of lignin may also unlock opportunities for the co-production of phenolics and related aromatic compounds via biorefineries for fine chemical and pharmaceutical applications[13] improving their cost-effectiveness.

Biodiesel is a clean burning and biodegradable fuel[14] which remains popular for meeting transportation energy requirements in Europe,[15] Asia,[16] the Americas[17] and Africa.[18] Commercial biodiesel is produced almost entirely via the liquid base catalysed transesterification of C_{14}-C_{20} triacylglyceride (TAG) components of lipids with C_1-C_2 alcohols[19] into fatty acid methyl esters (FAMEs) which constitute biodiesel. Higher alcohols have also been exploited[20] as they offer a less corrosive FAME with improved physical characteristics.[21] Isolation of the desired biodiesel product from homogeneous base catalysts (and unreacted mono- and di-alkyl glycerides and glycerol by-product) is necessary to circumvent saponification and emulsification side reactions and produce a high quality biofuel.[6] Heterogeneous, solid acid[22-24] and base catalysts offer facile FAME separation, eliminating the requirement for quenching steps and permitting continuous biodiesel production,[25] and a purer glycerol by-product stream for use as a commodity chemical in the food and cosmetics industry. Among solid base catalysts, hydrotalcites,[26-28] alkaline earth oxides[29-33] and alkali-doped mesoporous silicas[34] are good potential candidates for biodiesel formation under mild conditions. Hydrotalcites (of general formula $[M(II)_{1-x}M(III)_x(OH)_2]^{x+}(A_{n-x/n})\cdot mH_2O$) are a subset of microporous layered double hydroxides,[35] conventionally synthesised via co-precipitation from nitrates[36] in the presence of alkalis which are problematic due to NOx emissions[37] and in situ alkali leaching and consequent FAME contamination.[38-40] We recently reported an alkali/nitrate-free route to tunable Mg-Al hydrotalcite coatings via the direct reaction of $Mg(OCH_3)_2$ with a conventional, bulk alumina support.[41] While the resulting materials exhibited excellent Turnover Frequencies (TOFs) towards TAG transesterification, they suffer from a number of important drawbacks, namely: poor specific activity per unit mass towards bulky C_{18} substrates (0.042 $mmol.min^{-1}.g^{-1}$), low surface areas, and restricted (and disordered) pore architectures available through the use of pure alumina templates. In contrast, *hydrothermally stable* silica frameworks can be readily synthesised, offering *diverse pore interconnectivities and bi- or tri-modal pore networks*.[42-44]

Here we extend our previous methodology to create crystalline, catalytically active hydrotalcite coatings via a versatile two-step methodology, permitting (i) the first genesis of an ultrathin alumina adlayer over a complex (hierarchically

ordered) template, and (ii) facilitating its subsequent reaction with $Mg(OCH_3)_2$ to form a stoichiometric HT/MM-SBA-15 hydrotalcite catalyst. *This novel methodology opens the way to a new class of solid bases built upon the tunable interconnectivity and porosity afforded by underlying silica architectures*. The resulting nanocomposite combines the high surface area and excellent mass-transport characteristics of the parent silica, and solid basicity and transesterification performance of a pure hydrotalcite.

Catalyst synthesis

Synthesis of macroporous-mesoporous SBA-15 (MM-SBA-15)

An hierarchical macroporous-meosporous SBA-15 silica was prepared following the method of Dhainaut et al.[22] Briefly polystyrene beads synthesised via the emulsion polymerisation approach of Vaudreuil and co-workers[45] were added to an acidified, aqueous solution of Pluronic® P123 surfactant prior to the addition of tetramethoxysilane. The resulting gel was hydrothermally aged without agitation, and the solid obtained filtered, washed and dried at room temperature before calcination at 550 °C for 6 h in air.

Alumina grafting onto MM-SBA-15 (Al-MM-SBA-15)

The Al-MM-SBA-15 hierarchical framework employed the method of Landau and co-workers developed for MCM-41.[46] Aluminium-tri-sec-butoxide (14.5 g) was dissolved in anhydrous toluene (100 cm^3) at 85 °C with stirring. Triethylamine (2.1 cm^3) was added to this solution, followed by dried MM-SBA-15 (1 g). After 6 h stirring at 85 °C the solution was filtered under vacuum (~0.1 bar), with the recovered solid washed three times in toluene (100 cm^3). The alumina surface was then hydrolysed in ethanol (318 cm^3) containing water (1.6 cm^3) for 24 h at 25 °C with stirring, and the resulting solid recovered by vacuum filtration and washed with ethanol (300 cm^3) before drying at 80 ºC in a vacuum oven overnight. A three-step calcination sequence was utilised to form an alumina monolayer: the material was first heated to 250 °C for 1 h, then 400 °C for 1 h and finally 500 °C for 4 h (each ramp rate 1 $°C.min^{-1}$). Consecutive grafting cycles were undertaken employing an identical protocol in order to progressively build-up alumina monolayers over the silica surface, adjusting the quantities to maintain the initial Al:Si stoichiometry.

Synthesis of hydrotalcite-coated MM-SBA-15 (HT/MM-SBA-15)

Magnesium methoxide solution (8-10 wt% in methanol) was added to Al-MM-SBA-15 (400 mg, dried for 1 h at 80 °C), at the minimum quantity to form a homogeneous paste on mixing. After stirring for 15 min, the mixture was dried under vacuum at 80 °C for 1 h to remove excess methanol. The surface Mg:Al atomic ratio was tuned by adjusting the volume of magnesium methoxide (10.8 cm^3 for the MM-SBA-15). The resulting material was calcined at 450 °C for 15 h under 20 $cm^3.min^{-1}$ O_2 (ramp rate 1 $°C.min^{-1}$). After cooling to room temperature under N_2 (20 $cm^3.min^{-1}$), the powder was added to distilled water (50 cm^3 for every 300 mg of powder) in a 100 cm^3 round-bottomed pressure vessel and heated to 125 °C with stirring for 21 h. After cooling to room temperature, the final HT/MM-SBA-15 sample was filtered, washed with deionised water and dried in a vacuum oven overnight at 80 °C, before storage in a desiccator. This synthesis proved successful on the multi-gram scale. A conventional hydrotalcite reference material was prepared via our alkali-free, co-precipitation method from $Mg(NO_3)_2{\cdot}6H_2O$ and $Al(NO_3)_3{\cdot}9H_2O$ precursors,[26] with the Mg: Al atomic ratio tuned to match that of the MM-SBA-15.

Materials characterisation

Nitrogen porosimetry was undertaken on a Quantachrome Nova 1200 porosimeter. Multi-point BET surface areas were calculated over the relative pressure range 0.01–0.3. Pore diameters and volumes were calculated applying either the t-plot or BJH methods to the desorption isotherm. Powder XRD patterns were recorded on a PANalytical X'pertPro diffractometer fitted with an X'celerator detector and Cu Kα source; the Scherrer equation was used to calculate HT crystallite sizes. XPS was performed on a Kratos Axis HSi X-ray photoelectron spectrometer fitted with a charge neutraliser and magnetic focusing lens employing Al K_α monochromated radiation (1486.7 eV). Spectral fitting was performed using CasaXPS version 2.3.15. Base site densities were measured via CO_2 pulse chemisorption and subsequent temperature programmed desorption (TPD) on a Quantachrome ChemBET 3000 system coupled to an MKS Minilab QMS. SEM analysis was carried out on a Carl Zeiss EVO SEM fitted with an Oxford Instruments energy dispersive X-ray (EDX) analyser employing Oxford Instruments Inca Software. TGA was performed using a Stanton Redcroft STA780 thermal analyser.

Transesterification

The HT/MM-SBA-15 and conventional HT materials were tested as catalysts in the transesterification of triolein to form methyl trioleate (FAME) using a Radleys Starfish parallel reactor. Briefly, 50 mg of catalyst was added to 10 mmol of triolein using a 30:14:1 methanol:butanol:oil ratio; butanol was added as a co-solvent to help solubilise the triglyceride. In light of the significant differences in HT content between our conventional and SBA-15 coated materials, a common total mass of catalyst (rather than mass of hydrotalcite) was employed to ensure identical mixing characteristics within the reaction vessel. Reactions were carried out at 90 °C in a modified ACE™ 50 cm^3 round bottom pressure flask, with aliquots removed periodically from the reaction mixture for analysis on a Varian 450 GC with 8400 autosampler (programmable on-column injection onto a Phenomenex ZB-1HT column (15 m x 0.53 mm x 0.15 µm film thickness). Initial rates were calculated from the linear portion of the reaction profile during the first 60 min of the reaction. Turnover frequencies (TOFs) were determined by normalising rates to the total base site density from CO_2 chemisorption.

Results and Discussion

Characterisation of Al-MM-SBA-15

Alumina grafted silica (Al-MM-SBA-15) was first prepared as support for subsequent conversion to a high area, hierarchically ordered hydrotalcite coating. The alumina grafting process was repeated four times to obtain a uniform multilayer interface, with textural properties characterised after each grafting in order to examine the evolution of the alumina-silica interface. Low angle XRD and TEM of the parent MM-SBA-15 and the sequentially alumina grafted variants (**Figures S1-2**) confirmed the presence of ordered mesopores indicative of SBA-15.[47] Characteristic (100), (110) and (200) reflections were observed for all materials, indicative of the *p6mm* space group expected

for hexagonally arranged mesoporous channels.[48] Macropore incorporation shifted these reflections to higher angle relative to conventional mesoporous SBA-15, associated with a small contraction in the mesopore lattice parameter.[22] This contraction is attributed to curvature of the mesopore channels as they coalesce around the polystyrene bead template due to strong electrostatic interactions between the beads, block co-polymer and silica precursor. Long range, hexagonally ordered mesopores remained present for Al-MM-SBA-15 even following four consecutive grafting cycles.

Nitrogen porosimetry of the parent MM-SBA-15 and alumina grafted analogues confirmed that the mesoporosity intrinsic to the SBA-15 framework is maintained after each grafting cycle (**Figures S3a-b**). However, the BET surface area (and interconnecting micropore area from t-plot analysis), mean mesopore diameter, and total mesopore and micropore volumes decreased progressively with each grafting cycle (**Table 1**), consistent with an increasing thickness of conformal alumina overlayer uniformly distributed throughout the pore network.

Table 1. Porosimetry of Al-MM-SBA-15 as a function of grafting cycle

Material	Surface area[a] / $m^2.g^{-1}$	Mesopore volume[b] / $cm^3.g^{-1}$	Mesopore diameter[b] / nm	Micropore volume[c] / $cm^3.g^{-1}$	Micropore area[c] / $m^2.g^{-1}$
MM-SBA-15	473	0.66	3.9	0.079	166
Al-MM-SBA-15-1	332	0.48	4.0	0.024	58
Al-MM-SBA-15-2	271	0.47	4.0	0.013	33
Al-MM-SBA-15-3	240	0.46	3.7	0.007	19.3
Al-MM-SBA-15-4	201	0.45	3.7	0.004	13.5

[a]Multi-point BET method. [b]BJH mesopore volume and pore diameter from the desorption isotherm. [c]Calculated by t -plot method.

The surface of Al-MM-SBA-15 was subsequently investigated by XPS. Successful alumina grafting was confirmed by the presence of surface Al, with the Al:Si atomic ratio increasing monotonically with each cycle, reaching 22.3 wt% Al after four cycles. **Figure 1** compares the Al and Si 2p chemical environments for the parent and alumina grafted mesoporous silicas. The pure MM-SBA-15 exhibited a single Si 2p spin-orbit split doublet centred with Si $2p_{3/2}$ component at 103.1 eV binding energy associated with pure silica. Alumina grafting significantly attenuated the substrate signal consistent with a conformal (Frank-van der Merwe) growth mode, rather than the formation of 3-dimensional alumina islands. This attenuation was accompanied by the emergence of a second low binding energy doublet at 102.2 eV for Al-MM-SBA-15, which can only be associated with a new, interfacial silicon species. This hypothesis is supported by the observation of two distinct Al 2p spin-orbit doublets, at 73.8 eV and 74.7 eV. The former is consistent with pure alumina, and its intensity increases monotonically with grafting cycle relative to the high binding energy state, precisely as expected if the latter was associated with an interfacial alumina species. The opposing binding energy shifts for the interfacial Al and Si species are similar to those previously observed for alumina grafted SBA-15,[49] and can be understood in terms of their different Pauling electronegativities and associated induced dipoles mediated via the Al-O-Si bridges which increase and decrease the local initial state charge on interfacial Si and Al atoms respectively.

An estimate of the alumina film thickness may be obtained by comparing the experimentally determined Al surface density

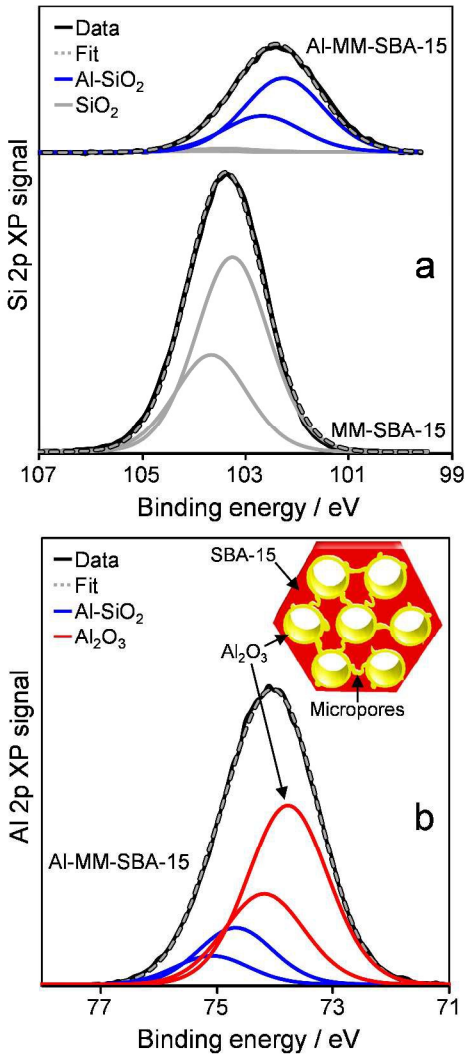

Figure 1. (a) Si and (b) Al 2p XP spectra of parent MM-SBA-15 and Al-MM-SBA-15 following four alumina grafting cycles.

(derived from porosimetry and XPS) with that for a crystalline alumina phase such as α-Al_2O_3, which exhibits a rhombohedral (4.75 Å x 4.75 Å) surface unit mesh containing three Al atoms within the (006) plane as shown in **Scheme 1**.[50] With a total surface area of 473 $m^2.g^{-1}$, a single α-Al_2O_3 monolayer covering the entire silica pore network would contain 0.0009 mol Al, equating to an Al loading of 24.3 wt%. This is close to the observed value of 22.3 wt%, and indicates that an alumina film approximately 0.7 monolayers thick (~0.17 nm) is formed following four grafting cycles, which would constrict the mesopores by 0.34 nm relative to the parent MM-SBA-15, in excellent agreement with the observed pore diameter decrease of 0.3 nm seen in **Table 1**.

Characterisation of HT/MM-SBA-15

Powder XRD diffraction patterns for the methoxide functionalised Al-MM-SBA-15 material prepared via four alumina grafting cycles (HT/MM-SBA-15), and a reference bulk HT sample prepared by conventional alkali-free co-precipitation (ConvHT) are shown in **Figure 2**. The HT/MM-

SBA-15 sample shows a diffraction pattern characteristic of a pure HT phase, very similar to that observed for the ConvHT

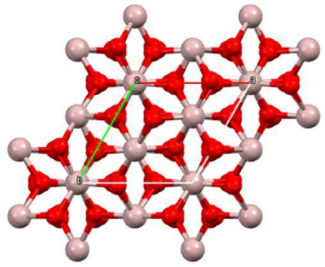

Scheme 1. Crystal structure of α-alumina with primitive cell highlighted.[50]

standard, but with broader reflections indicative of significantly smaller crystallite sizes (as anticipated in light of the highly dispersed alumina substrate, which by inference appears to undergo little restructuring during the crystallisation process) and turbostratic disorder.[51] There was no evidence for brucite[52] and only a single weak reflection likely associated with trace MgO. This confirms the successful synthesis of a hydrotalcite phase through direct reaction of a pre-formed, ultrathin alumina film and magnesium methoxide from solution.

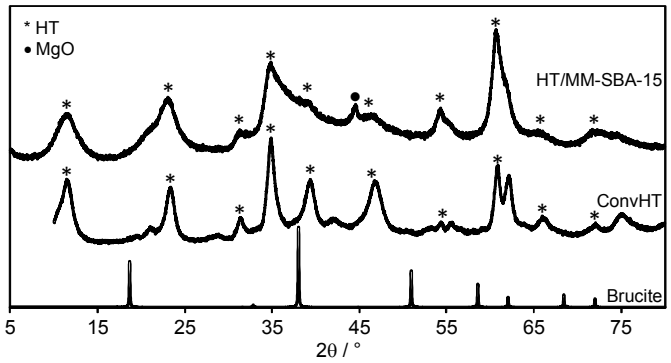

Figure 2. Powder XRD patterns for HT/MM-SBA-15 and a conventional HT standard (offset for clarity)

Crystallite sizes determined using the Scherrer equation, interlayer spacings, lattice parameters and Mg:Al ratios determined using Vegard's law (**Figure S4**) are reported in **Table 2**. The composition, lattice parameter and interlayer spacings of the HT/MM-SBA-15 material were almost identical to that of the ConvHT, confirming that the hydrotalcite phase formed at the surface of the hierarchical silica support was essentially indistinguishable from that of obtained by traditional synthetic methods, but with a surface area around five times higher. However, the significant difference in microporous crystallites size is expected to hinder accessibility of reactatns to active sites within the ConvHT interlayers relative to the HT/MM-SBA-15 sample whose dimensions suggest a hydrotalcite bilayer wherein a far greater proportion of base sites reside on exposed surfaces.

Textural properties of the HT/MM-SBA-15 material are compared with those of the Al-MM-SBA-15 precursor in **Figure 3**. Nitrogen porosimetry evidences retention of mesopore and macropore character within the adsorption/desorption isotherms following HT crystallisation, although their demarcation is not as clear as for Al-MM-SBA-15 (**Figure S3**), while **Table S1** shows virtually no change in either the mesopore volume or mean mesopore diameter upon reaction of the alumina adlayer with $Mg(OCH_3)_2$. This suggests that either extremely thin HT crystallites are formed throughout the bimodal pore network (consistent with XRD), or that hydrotalcite formation is confined to the macropores. The latter would be expected to hinder accessibility of the mesopores (for which macropores serve as the principal conduits), and hence reduce both the mesopore volume and total surface area, in contrast to the observed values reported in **Table S1**.

Table 2. Crystallographic properties of HT/MM-SBA-15 and ConvHT

Material	Crystallite size / nm[a]	Interlayer spacing / nm[a]	Lattice parameter / nm[a]	Mg:Al ratio[b]
HT/MM-SBA-15	1.18	0.76	0.305	2.21:1
ConvHT	6.2	0.77	0.305	1.95:1

[a]Calculated using Scherrer equation; [b]Determined from lattice parameter using Vegard's Law.

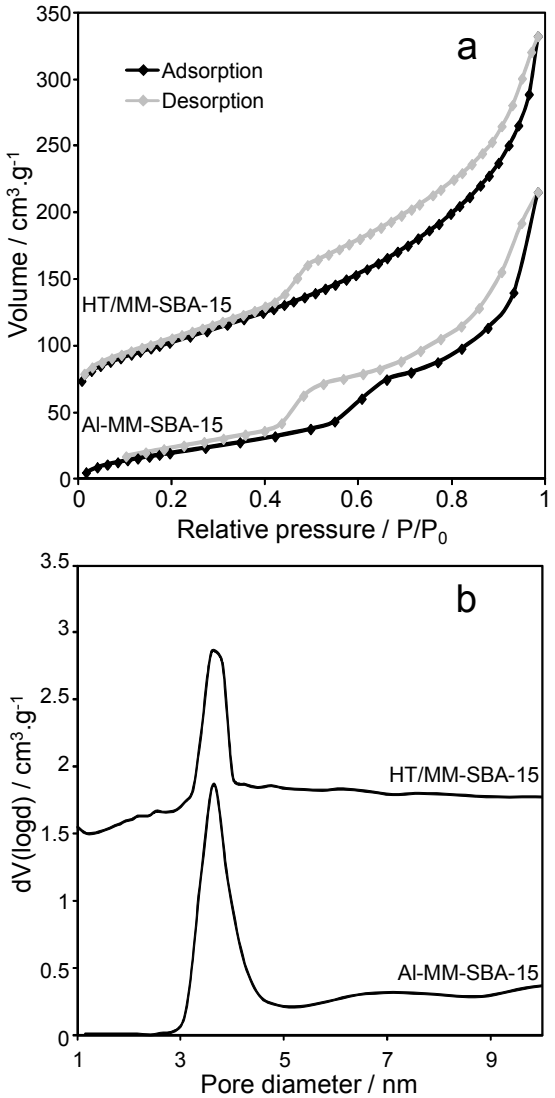

Figure 3. (a) N_2 adsorption-desorption isotherms and (b) BJH pore size distributions for Al-MM-SBA-15 precursor and HT/MM-SBA-15 (offset for clarity).

SEM of the HT/MM-SBA-15 (**Figure 4**) confirms the macropore network present within the parent MM-SBA-15 support is retained throughout the material after hydrothermal treatment, a measure of the excellent stability of silica frameworks towards high temperature water, and conditions that a comparable pure hierarchical alumina structure would be unlikely to survive. TEM shows macropores are decorated with high aspect ratio hydrotalcite nanocrystallites. Thermogravimetric analysis confirms the excellent thermal stability of the HT/MMSBA-15 (**Figure S5**), with only a small 10 % weight loss between 70 and 220 °C, associated with the desorption of physisorbed water from the HT surface and water from within the interlayers,[53] and a 5 % loss between 250 and 350 °C attributed to hydroxide anions in the brucite-like layers.[54] EDX elemental analysis of the HT/MM-SBA-15 yields an overall Mg:Al atomic ratio of 2.2:1, in good agreement with that derived from Vegard's law in **Table 2**, and a total Mg content of 19.8 wt% i.e. a quarter that of a bulk hydrotalcite of comparable Mg:Al ratio,[26] consistent with the formation of hydrotalcite nanocrystals approximately 1 nm thick relative to silica walls around 4-5 nm thick in the MM-SBA-15 support.[49]

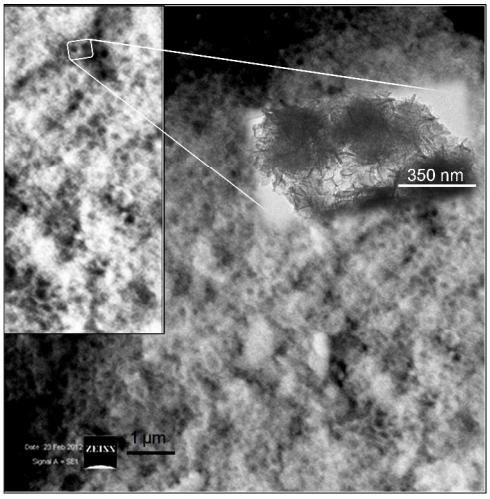

Figure 4. SEM and TEM micrographs of HT/MM-SBA-15. Insets highlight macropore network and hydrotalcite crystallites decorating macropores.

Surface base properties of the HT/MM-SBA-15 and ConvHT bulk reference materials were assessed by temperature-programmed desorption of CO_2-saturated samples, presented in **Figure S6**. The desorption profile of HT/MM-SBA-15 mirrors that of the bulk hydrotalcite, both exhibiting a single desorption feature around 340 °C indicative of moderate strength base sites, albeit spanning a broader temperature range and hence distribution of basicity for the HT/MM-SBA-15.Total base site densities for the HT/MM-SBA-15 and ConvHT materials were 6.4×10^{18} and 8.6×10^{19} m^{-2} respectively, although one should recall that a large proportion of sites present within the interlayers of the bulk hydrotalcite structure may be inaccessible to sterically-demanding substrates. These results confirm that high aspect ratio hydrotalcite crystallites formed over the hierarchical silica support possess similar intrinsic basicity to conventional co-precipitated analogues.

Surface analysis of HT/MM-SBA-15 yielded a Mg:Al atomic ratio of 2.21 and Mg content of 16.7 wt%, both very similar to values determined by EDX, evidencing uniform incorporation of Mg into the alumina film throughout the pore network of the Al-MM-SBA-15 precursor. Si 2p XP spectra shown in **Fig. 5a** reveal that hydrotalcite formation was accompanied by attenuation of the interfacial alumina species, and concomitant appearance of a new low binding energy

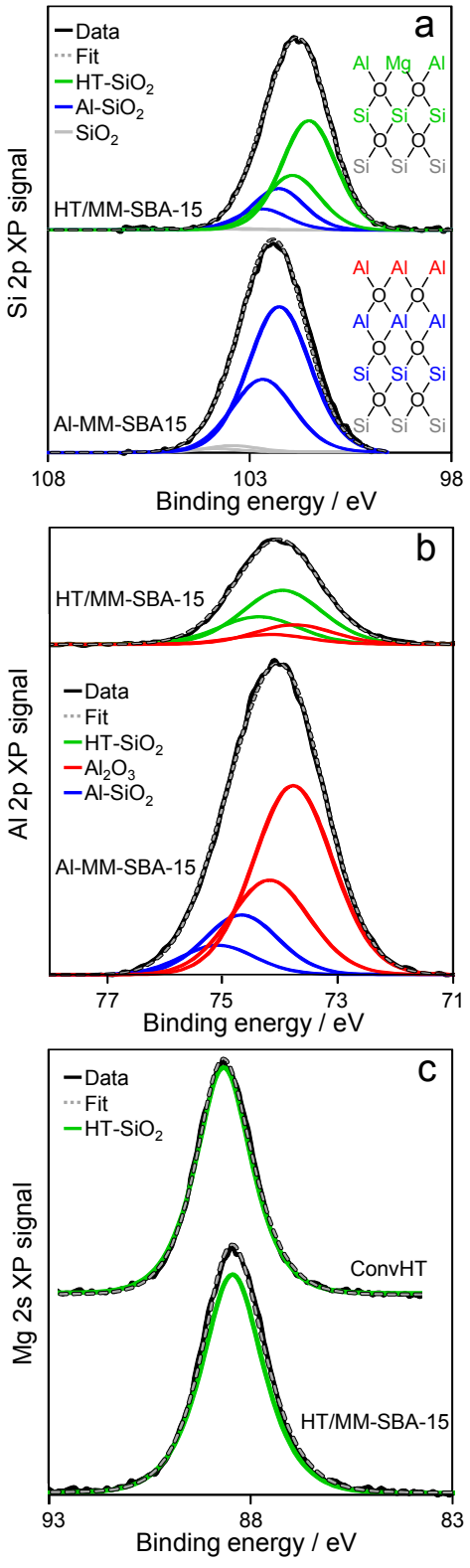

Figure 5. (a) Si 2p and (b) Al 2p, and (c) Mg 2s XP spectra of Al-MM-SBA-15 precursor and HT/MM-SBA-15.

chemical environment at 101.5 eV. The latter suggests that interfacial silicon atoms are now bound (through oxygen bridges) to a less polarising adlayer relative to alumina, consistent with the exchange of Al^{3+} for Mg^{2+} cations. **Fig. 5b** shows analogous changes in the Al chemical environment, with attenuation of the pure (and interfacial) alumina adlayer, and emergence of a high energy Al state ~74 eV, consistent with the introduction of Mg^{2+} cations into the grafted alumina film during hydrotalcite formation. The corresponding Mg 2s XP spectrum of HT/MM-SBA-15 presents a single chemical environment around 88.5 eV. In summary, over 75 % of the MM-SBA-15 silica surface is contacted with a hydrotalcite phase, and a similar proportion of the initially grafted alumina adlayer in Al-MM-SBA-15 is converted into hydrotalcite.

Transesterification of triglycerides

In order to establish the catalytic efficacy of the HT film encapsulating the hierarchical silica template, the HT/MM-SBA-15 material was screened in the transesterification of glyeryl triolein, a bulky C_{18} triglyceride that is a major component on oilseed feedstocks, with methanol for FAME (biodiesel) production. The resulting reaction profiles for HT/MM-SBA-15 and the co-precipitated ConvHT analogue are shown in **Figure 6**. Transesterification proceeded rapidly over both catalysts during the first hour of reaction before slowing dramatically, to give limiting conversions of 34 % and 64 % for HT/MM-SBA-15 and ConvHT respectively. While the absolute FAME productivity of the bulk hydrotalcite is clearly superior,

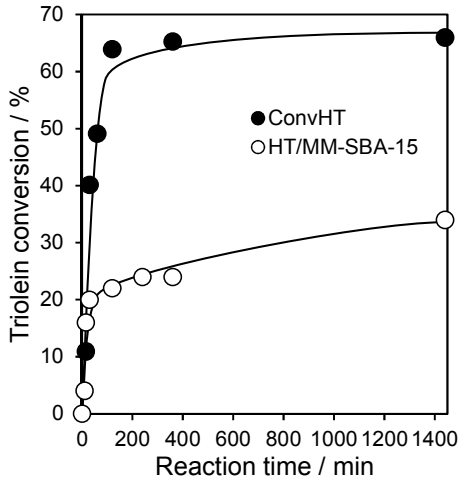

Figure 6. Triolein conversion to methyl trioleate via transesterification with methanol (1:30 molar ratio) at 90 °C over HT-MM-SBA-15 and a conventional HT standard.

it is important to recall that the HT/MM-SBA-15 only contains a thin hydrotalcite coating and the majority of this catalyst is composed of inert silica. A fairer comparison of the relative catalytic performance is obtained from their initial rates of triolein conversion and Turnover Frequencies (TOFs) normalised per base site utilising the CO_2 TPD measurements. This reveals a common initial rate of 1 $mmol.g_{catalyst}^{-1}.min^{-1}$, however one must recall that the HT/MM-SBA-15 material only contains one quarter of the amount of hydrotalcite present within the bulk ConvHT material, hence the rate normalised per mass of hydrotalcite is four times higher for HT/MM-SBA-15 catalyst. Since the base site density of the coated hydrotalcite is also ~34 % lower than that of its bulk counterpart, the rate enhancement *per base site* of the coated material is higher still, translating to TOFs of 7.6 min^{-1} for the bulk ConvHT standard versus 66 min^{-1} for HT/MM-SBA-15. Hydrotalcites prepared via conventional co-precipitation are among the most widely-used catalysts for triglyceride transesterification to FAME, hence the nine-fold rate enhancement observed for our HT/MM-SBA-15 material provides a striking benchmark of its exceptional performance. While the magnitude of this enhancement does fall at longer reaction times, likely due to partial deactivation of the coating, the HT/MM-SBA-15 remains three times as active per base site as the bulk hydrotalcite, even after 1400 min reaction.

Since the intrinsic base strength of active sites within the conventional and hierarchical hydrotalcite catalysts is the same (common CO_2 desorption temperatures, **Figure S6**), we attribute this nine-fold rate enhancement of HT/MM-SBA-15 to superior mass-transport characteristics of the macroporous-mesoporous architecture. Indeed, the magnitude of the HT/MM-SBA-15 enhancement with respect to the ConvHT standard is comparable to that previously reported for a macroporous pure HT material,[28] but affords a far more flexible and hydrothermally stable framework than the latter synthesis.

Conclusions

Sequential, wet-chemical surface modification of nanostructured silicas with Al and Mg precursors offers a versatile route to the preparation of high area, tailored solid base hydrotalcite catalysts. Stepwise grafting and thermal processing of aluminium-tri-sec-butoxide results in a uniform alumina monolayer throughout the bimodal macropore-mesopore network. Subsequent reaction with $Mg(OCH_3)_2$ affords stoichiometric incorporation of aluminium from the alumina adlayer into ~1 nm Mg_2Al hydrotalcite crystallites, which possess identical basicity as a co-precipitated, bulk hydrotalcite. In contrast to bulk (monomodal) alumina templates, the development of a silica based methodology results in HT/MM-SBA-15 catalyst exhibits similar specific mass activity in the transesterification of glyceryl triolein with methanol as a bulk hydrotalcite, despite containing only a small fraction of the number of active sites, indicating far greater active site accessibility to the bulky TAG reactant. The latter conclusion is supported by a nine-fold enhancement in the TOF per base site for the hierarchical hydrotalcite, indicating the majority of base sites in HT/MM-SBA-15 reside at the external surface of nanoscale crystallites within the meso- and macropores, rather than within the microporous interlayers of conventional hydrotalcites. Our methodology is readily extendable to diverse silica architectures and other metal oxides, opening up opportunities for the facile introduction of hydrotalcite solid basicity into complex two- or three-dimensional materials, e.g. membranes and monoliths, for catalysis and sorption applications.

Acknowledgements

We thank the EPSRC (EP/G007594/4) for financial support and a Leadership Fellowship (AFL) and studentship (JJC), and the Royal Society for the award of an Industry.

Notes and references

[a] School of Chemistry, Cardiff University, Cardiff CF10 3AT, UK.

[b] European Bioenergy Research Institute, Aston University, Birmingham B4 7ET, UK. a.f.lee@aston.ac.uk; +44 121 2044036.

Electronic Supplementary Information (ESI) available: Full material synthesis and characterisation. See DOI: 10.1039/c000000x/

1. *International Energy Outlook 2013*, Report DOE/EIA-0484(2013), 2013.
2. R. Luque, L. Herrero-Davila, J. M. Campelo, J. H. Clark, J. M. Hidalgo, D. Luna, J. M. Marinas and A. A. Romero, *Energy & Environmental Science*, 2008, 1, 542-564.
3. BP, *BP Energy Outlook 2030*, 2011.
4. F. Danielsen, H. Beukema, N. D. Burgess, F. Parish, C. A. BrÜHl, P. F. Donald, D. Murdiyarso, B. E. N. Phalan, L. Reijnders, M. Struebig and E. B. Fitzherbert, *Conservation Biology*, 2009, 23, 348-358.
5. W. M. J. Achten, L. Verchot, Y. J. Franken, E. Mathijs, V. P. Singh, R. Aerts and B. Muys, *Biomass & Bioenergy*, 2008, 32, 1063-1084.
6. T. M. Mata, A. A. Martins and N. S. Caetano, *Renewable and Sustainable Energy Reviews*, 2010, 14, 217-232.
7. R. Pate, G. Klise and B. Wu, *Applied Energy*, 2011, 88, 3377-3388.
8. A. Demirbas, *Energy Policy*, 2007, 35, 4661-4670.
9. P. M. Mortensen, J. D. Grunwaldt, P. A. Jensen, K. G. Knudsen and A. D. Jensen, *Applied Catalysis A: General*, 2011, 407, 1-19.
10. H. Jahangiri, J. Bennett, P. Mahjoubi, K. Wilson and S. Gu, *Catalysis Science & Technology*, 2014, 4, 2210-2229.
11. F. Trippe, M. Fröhling, F. Schultmann, R. Stahl, E. Henrich and A. Dalai, *Fuel Processing Technology*, 2013, 106, 577-586.
12. C. S. K. Lin, L. A. Pfaltzgraff, L. Herrero-Davila, E. B. Mubofu, S. Abderrahim, J. H. Clark, A. A. Koutinas, N. Kopsahelis, K. Stamatelatou, F. Dickson, S. Thankappan, Z. Mohamed, R. Brocklesby and R. Luque, *Energy & Environmental Science*, 2013, 6, 426-464.
13. M. P. Pandey and C. S. Kim, *Chemical Engineering & Technology*, 2011, 34, 29-41.
14. G. Knothe, *Topics in Catalysis*, 2010, 53, 714-720.
15. K. Bozbas, *Renewable and Sustainable Energy Reviews*, 2008, 12, 542-552.
16. M. H. M. Ashnani, A. Johari, H. Hashim and E. Hasani, *Renewable and Sustainable Energy Reviews*, 2014, 35, 244-257.
17. J. C. Bergmann, D. D. Tupinambá, O. Y. A. Costa, J. R. M. Almeida, C. C. Barreto and B. F. Quirino, *Renewable and Sustainable Energy Reviews*, 2013, 21, 411-420.
18. B. Amigun, J. K. Musango and W. Stafford, *Renewable and Sustainable Energy Reviews*, 2011, 15, 1360-1372.
19. A. F. Lee, J. A. Bennett, J. C. Manayil and K. Wilson, *Chemical Society Reviews*, 2014, DOI: 10.1039/C4CS00189C.
20. J. Geuens, J. M. Kremsner, B. A. Nebel, S. Schober, R. A. Dommisse, M. Mittelbach, S. Tavernier, C. O. Kappe and B. U. W. Maes, *Energy & Fuels*, 2007, 22, 643-645.
21. G. Knothe, *Fuel Processing Technology*, 2005, 86, 1059-1070.
22. J. Dhainaut, J.-P. Dacquin, A. F. Lee and K. Wilson, *Green Chemistry*, 2010, 12, 296-303.
23. J. P. Dacquin, A. F. Lee, C. Pirez and K. Wilson, *Chemical Communications*, 2012, 48, 212-214.
24. Zillillah, T. A. Ngu and Z. Li, *Green Chemistry*, 2014, 16, 1202-1210.
25. K. Wilson and A. F. Lee, *Catalysis Science & Technology*, 2012, 2, 884-897.
26. D. G. Cantrell, L. J. Gillie, A. F. Lee and K. Wilson, *Applied Catalysis A: General*, 2005, 287, 183-190.
27. Y. Liu, E. Lotero, J. G. Goodwin and X. Mo, *Applied Catalysis A: General*, 2007, 33, 138-148.
28. J. J. Woodford, J.-P. Dacquin, K. Wilson and A. F. Lee, *Energy & Environmental Science*, 2012, 5, 6145-6150.
29. R. S. Watkins, A. F. Lee and K. Wilson, *Green Chemistry*, 2004, 6, 335-340.
30. K. Wilson, C. Hardacre, A. F. Lee, J. M. Montero and L. Shellard, *Green Chemistry*, 2008, 10, 654-659.
31. J. M. Montero, P. Gai, K. Wilson and A. F. Lee, *Green Chemistry*, 2009, 11, 265-268.
32. M. Verziu, B. Cojocaru, J. Hu, R. Richards, C. Ciuculescu, P. Filip and V. I. Parvulescu, *Green Chemistry*, 2008, 10, 373-381.
33. J. J. Woodford, C. M. A. Parlett, J.-P. Dacquin, G. Cibin, A. Dent, J. Montero, K. Wilson and A. F. Lee, *Journal of Chemical Technology & Biotechnology*, 2014, 89, 73-80.
34. M. C. G. Albuquerque, I. Jimenez-Urbistondo, J. Santamaria-Gonzalez, J. M. Merida-Robles, R. Moreno-Tost, E. Rodriguez-Castellon, A. Jimenez-Lopez, D. C. S. Azevedo, C. L. Cavalcante, Jr. and P. Maireles-Torres, *Applied Catalysis a-General*, 2008, 334, 35-43.
35. S. J. Mills, A. G. Christy, J. M. R. Genin, T. Kameda and F. Colombo, *Mineral. Mag.*, 2012, 76, 1289-1336.
36. Y. Xi and R. J. Davis, *Journal of Catalysis*, 2009, 268, 307-317.
37. M. Behrens, Ki, F. Girsgdies, I. Kasatkin, F. Hermerschmidt, K. Mette, H. Ruland, M. Muhler and R. Schlogl, *Chemical Communications*, 2011, 47, 1701-1703.
38. D. M. Alonso, R. Mariscal, M. L. Granados and P. Maireles-Torres, *Catalysis Today*, 2009, 143, 167-171.
39. M. Di Serio, R. Tesser, L. Casale, A. D'Angelo, M. Trifuoggi and E. Santacesaria, *Topics in Catalysis*, 2010, 53, 811-819.
40. Y. C. Sharma, B. Singh and J. Korstad, *Fuel*, 2011, 90, 1309-1324.
41. J. J. Creasey, A. Chieregato, J. C. Manayil, C. M. A. Parlett, K. Wilson and A. F. Lee, *Catalysis Science & Technology*, 2014, 4, 861-870.
42. Y. Wan and Zhao, *Chemical Reviews*, 2007, 107, 2821-2860.
43. Z. Li, X. Wei, T. Ming, J. Wang and T. Ngai, *Chemical Communications*, 2010, 46, 8767-8769.
44. C. M. A. Parlett, K. Wilson and A. F. Lee, *Chemical Society Reviews*, 2013, 42, 3876-3893.
45. S. Vaudreuil, M. Bousmina, S. Kaliaguine and L. Bonneviot, *Advanced Materials*, 2001, 13, 1310-1312.
46. M. V. Landau, E. Dafa, M. L. Kaliya, T. Sen and M. Herskowitz, *Microporous and Mesoporous Materials*, 2001, 49, 65-81.
47. A. Y. Khodakov, V. L. Zholobenko, R. Bechara and D. Durand, *Microporous and Mesoporous Materials*, 2005, 79, 29-39.
48. D. Zhao, Q. Huo, J. Feng, B. F. Chmelka and G. D. Stucky, *Journal of the American Chemical Society*, 1998, 120, 6024-6036.
49. C. M. A. Parlett, L. J. Durndell, A. Machado, G. Cibin, D. W. Bruce, N. S. Hondow, K. Wilson and A. F. Lee, *Catalysis Today*, 2014, 229, 46-55.
50. E. N. Maslen, V. A. Streltsov, N. R. Streltsova, N. Ishizawa and Y. Satow, *Acta Crystallographica Section B*, 1993, 49, 973-980.
51. G. Thomas and P. V. Kamath, *J Chem Sci*, 2006, 118, 127-133.
52. A. V. G. Chizmeshya, M. J. McKelvy, R. Sharma, R. W. Carpenter and H. Bearat, *Materials Chemistry and Physics*, 2003, 77, 416-425.

53. H. C. Greenwell, P. J. Holliman, W. Jones and B. V. Velasco, *Catalysis Today*, 2006, 114, 397-402.
54. S. Abelló, F. Medina, D. Tichit, J. Pérez-Ramírez, J. C. Groen, J. E. Sueiras, P. Salagre and Y. Cesteros, *Chemistry – A European Journal*, 2005, 11, 728-739.